Velocity Model Building Using Tilted Orthorhombic Depth Imaging for Full Azimuth Seismic Data

Yunfeng (Fred) Li, Qiaofeng Wu, and Chuen-Song Chen

CGG, 10300 Town Park Dr., Houston, Texas 77072, U.S.A.

ABSTRACT

Wide-azimuth (WAZ) data have been acquired in most of the deepwater blocks in the Gulf of Mexico. Compared with isotropic and vertical transverse isotropic (VTI) imaging, tilted transverse isotropic (TTI) prestack depth imaging generally provides flatter common image gathers (CIGs) for WAZ data, improves image focusing, and significantly reduces well/seismic misties. However, the presence of significant tectonic stress or uneven stress can cause fractures in thin-bed layers, which results in a directional velocity variation for seismic wave propagation, or azimuthal anisotropy. In these cases, the transverse isotropic assumption is insufficient to explain conflicting residual moveouts among CIGs of different azimuths from TTI imaging. A more general anisotropic model, tilted orthorhombic (TOR), is needed to cope with azimuthal velocity variation in these complex geological settings. Full azimuth (FAZ) data provide a better opportunity to derive the parameters of a tilted orthorhombic model. This paper shows the methodology and effectiveness of the TOR model building with a FAZ data in the deepwater Gulf of Mexico.

INTRODUCTION

Rock heterogeneity and horizontal stratification is one component of the local stress field (Dewey et al., 2006; Schoenbergm and Helbig, 1997; Bakulin et al., 2000). This stratification typically implies transverse isotropy (TI). Vertical transverse isotropic (VTI) or tilted transverse isotropic (TTI) imaging are simplified anisotropic representations and assume that wave propagation speeds are the same in the transverse plane (Thomsen, 1986). Recently, TTI imaging has become a standard practice in the deepwater Gulf of Mexico to resolve the anisotropic effects of wave propagation in salt-withdrawal minibasins (Huang et al., 2009). However, in some complex overburden areas, where significant uneven stress and fractures exist (Schoenberg and Helbig, 1997), one commonly observes inconsistent residual moveout in common images gathers (CIGs) among different azimuths despite our best TTI practice.

Generally, tilted orthorhombic (TOR) anisotropy, which represents parallel-aligned fractures normally embedded in tilted thin sedimentary layers (Williams and Jenner, 2002; Lynn and Michelena, 2011), is a less-restricted assumption and can be applied to more complicated geological formations. A TTI model needs five parameters, and a TOR model is represented by nine parameters (Scott et al., 1991; Tsvankin, 1997) as shown in Figure 1. Deriving a set of reliable TOR parameters is challenging;

however, it becomes feasible due to the advances in acquisition and anisotropic imaging technology. First, wide azimuth (WAZ) data have been acquired in most of the deepwater blocks in the Gulf of Mexico, and full azimuth (FAZ) data are quickly being used to improve subsurface illumination (Dickinson et al 2010; Bowling et al., 2010; F. Mandroux, 2012, personal communication). FAZ data provide abundant azimuthal information for deriving these nine parameters. Additionally, during the last couple of years, ray tracing and tomography (Han and Xu, 2012; Li et al., 2012), Kirchhoff and beam migration (Mensch et al., 1998; Xie et al., 2011; Birdus et al., 2012; Zhou et al., 2011), and wave migration (Alkhalifah, 2003; Zhu and Tsvankin, 2007; Zhang and Zhang, 2011; Fowler and King, 2011) have been developed to address TOR anisotropy.

In this paper, we demonstrate the procedure for TOR model building—the initialization of a TOR depth model and the implementation of TOR tomography. In order to show the effectiveness of the TOR model building with full-azimuth data, we chose a study area located in Keathley Canyon, in the central Gulf of Mexico, which is interior to the Sigsbee Escarpment and features complex salt structures, such as reverse faults, carapaces, and faulted fold structures in the suprasalt region. Fractures are expected to generally parallel fault strikes and leads to azimuthal anisotropy. With an FAZ dataset, we demonstrate that (1) FAZ data are more effective in detecting azimuthal anisotropy than WAZ data and (2) TOR model building with FAZ can better resolve anisotropy in the overburden in the presence of fractures and uneven stress. The fast velocity direction in the TOR model is consistent with the strikes of fractures in our study area. As a result, TOR reverse time migration (RTM) with FAZ data improves the imaging of overburden structures, and the better defined overburden leads to improvement in salt geometry and provides better subsalt images.
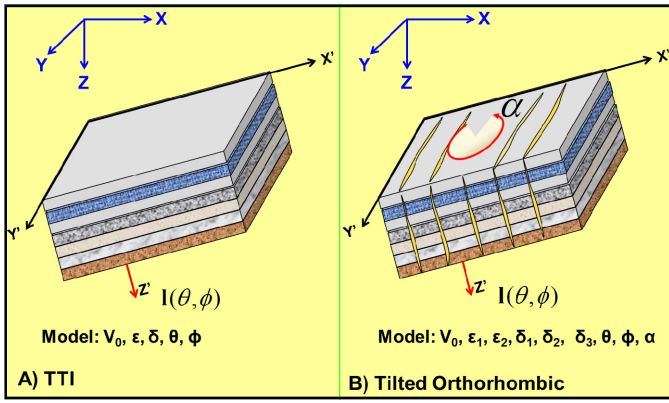
Figure 1. Comparison of TTI and TOR media. (A) TTI: stress and wave are symmetrical in [x´, y´] plane with one symmetry axis. (B) TOR: Stress varies on the fracture plane with three orthogonal symmetry planes defined by angles (θ, φ, and α).

METHOD

Estimation of Initial Tilted Orthorhombic Model and Tilted Orthorhombic Tomography

As shown in Figure 1, there are nine parameters to be estimated for the TOR model (v_0, ε_1, δ_1, ε_2, δ_2, δ_3, θ, φ, and α). v_0 is the velocity along the z direction, which is assumed to be the slowest propagation direction. (ε_1 and δ_1) are defined in the symmetry plane [y´, z´], and (ε_2 and δ_2) are defined in the symmetry plane [x´, z´]. Without loss of generality, we assume $\varepsilon_1 > \varepsilon_2$. As in conventional TTI, θ and φ are defined by the rotation of the vertical axis at each spatial location. The rotation angle of the elastic tensor in the [x´, y´] plane, α, is identical to the angle between the crack orientation and the y´ axis in the TTI local coordinate system. Of the nine parameters in the TOR model, v_0, ε_1, ε_2, and α are usually the most sensitive parameters to TOR tomography updates. Herein we describe how we initialize the TOR model.

Starting with conventional TTI model building using FAZ data, a TTI model (v_0, ε_0, δ_0, θ, and φ) can be obtained after several iterations of TTI tomography. Moveout discrepancies on CIGs among different azimuths will be observed in TOR media, which indicates that one TTI model cannot flatten the CIGs for all of the azimuths. We begin the process of building the initial TOR model by first obtaining v_0, θ, and φ. v_0 is taken from the TTI model and smoothed to ensure it is free of anomalies and has an overall tie to wells (check shot, markers). Parameters θ and φ are directly inherited from the TTI model. To derive the remaining parameters (ε_1, δ_1, ε_2, δ_2, δ_3, and α), we fix v_0, θ, and φ, then perform TTI tomographic updates of ε_β and δ_β for each individual azimuth (one model per azimuth) to flatten CIGs, where β represents one individual azimuth as shown in Figure 2. For each individual azimuth, the apparent velocity in the TOR plane [x´, y´] is:

$$v_\beta{}^2 = \left(1 + 2\varepsilon_\beta\right) \times v_0{}^2 \qquad (1)$$

Given a full azimuth coverage, orthorhombic parameters ε_1, ε_2, δ_1, δ_2, and δ_3 can be simultaneously obtained by fitting the complex orthorhombic curvature in the subsurface plane [x´, y´]. Thus, for the purpose of building the initial model, we assume that the distribution of velocities in the [x´, y´] plane is close to an ellipse. Then, we can find a simple, best-fit ellipse to obtain an initial orthorhombic model. We use a residual function χ of the ellipse defined as:

$$\chi^2 = \sum_\beta \left[1 - \left(\frac{\left(v_\beta \cos(\beta - \alpha)\right)^2}{v_0^2(1 + 2\varepsilon_1)} + \frac{\left(v_\beta \sin(\beta - \alpha)\right)^2}{v_0^2(1 + 2\varepsilon_2)} \right) \right]^2 \qquad (2)$$
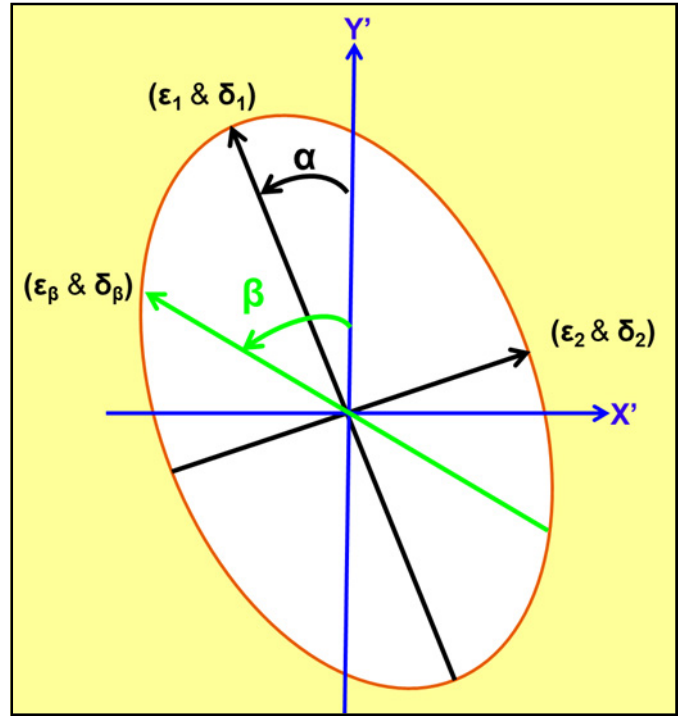

Figure 2. In the subsurface TOR plane [x´, y´], a is the rotation angle of the elastic tensor in the [x´, y´] plane, which indicates the major axis (ε_1 and δ_1) of the elliptic velocity system. (ε_2 and δ_2) is its minor axis. β is one of the multiple azimuths, and its apparent velocity in the TOR [x´, y´] plane locates on the elliptic velocity system.

For TOR media with a minimum of three azimuths of data, the initial ε_1, ε_2, and α can be obtained by minimizing the χ in Equation 2. δ_1 and δ_2 can be fitted as well from the elliptic assumption. δ_3 can be derived by the acoustic approximation in the orthorhombic system (Han and Xu, 2012). At this stage, we have derived initial models for the nine TOR attributes (v_0, ε_1, δ_1, ε_2, δ_2, δ_3, θ, φ, and α).

With orthorhombic ray tracing (Han and Xu, 2012), Kirchhoff migration is performed with the initial models to generate FAZ CIGs, from which residual curvatures are picked. Similar to the method used in TTI tomography (Huang et al., 2007), we set up a sparse linear system based on the invariant of travel time:

$$\frac{dt}{dz}\Delta z = -\sum l_i \left(\frac{\partial s_{\vec{n}}}{\partial s}\Delta s + \frac{\partial s_{\vec{n}}}{\partial \varepsilon_1}\Delta\varepsilon_1 + \frac{\partial s_{\vec{n}}}{\partial \varepsilon_2}\Delta\varepsilon_2 \right) \qquad (3)$$

Here, Δz is the difference between the picked event depth and the true depth, s is the slowness, and is the l_i length of the ray in each cell of the velocity model. TOR model updates (v_0 only; ε_1 and ε_2; or v_0, ε_1, and ε_2) are conducted by solving this linear system (Huang et al., 2007). If any well information is available, such as misties, this information can be incorporated to constrain the TOR tomographic output.

APPLICATION

Full Azimuth Towed Streamer Data in the Central Gulf of Mexico

We apply the TOR methodology to an area in Keathley Canyon, in the central Gulf of Mexico (Fig. 3A), which is interior to the Sigsbee Escarpment and features complex salt structures. A seismic section through the area reveals faults, carapaces and faulted fold structures in the suprasalt region (Fig. 3B). Fractures are expected to generally parallel fault strikes in the area (Hilley
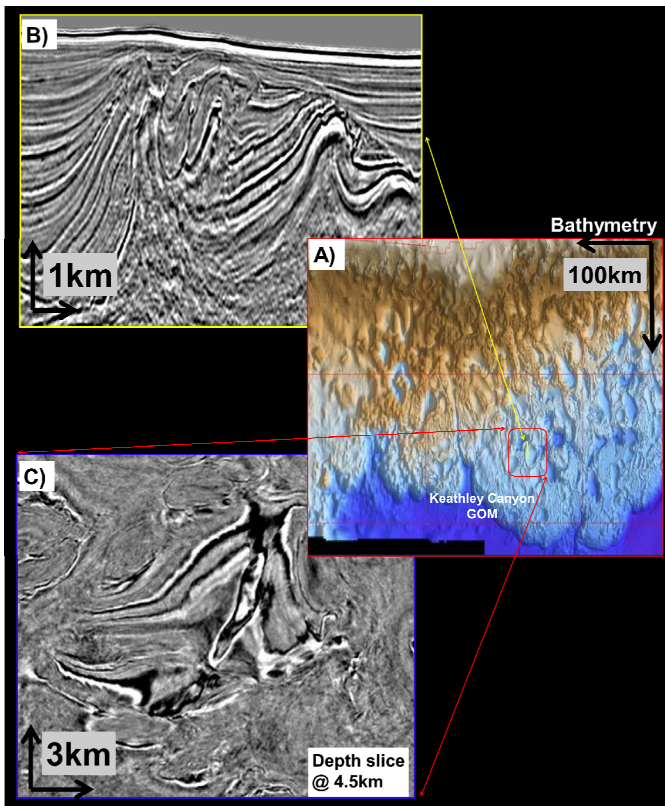
Figure 3. **(A) Location of the FAZ survey in Keathley Canyon, Gulf of Mexico. (B) A seismic section across the complex overburden area reveals a thrusted fold belt in the suprasalt region. (C) The depth slice at 4.5 km.**
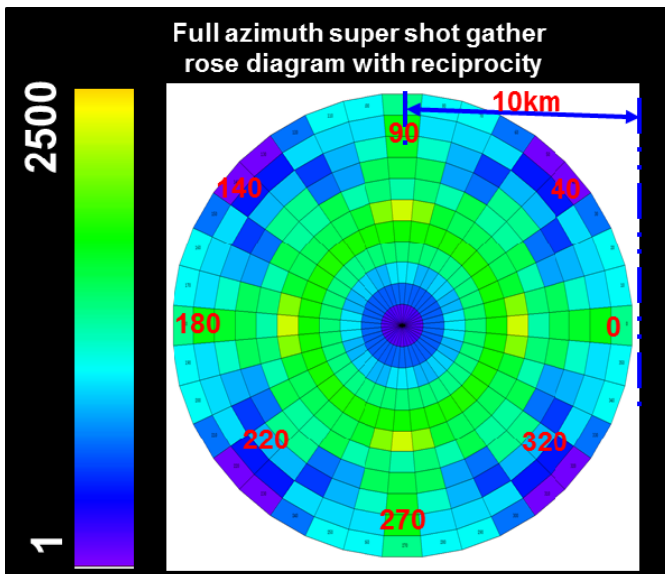

Figure 5. **(A) Definition of seven azimuth-offset sectors of the FAZ survey. (B) Definition of snail CIGs (Lecerf et al., 2009). (C) TTI seven-azimuths CIG panels. (D) TTI snail CIGs.**

Figure 4. **Rose diagram shows offset and azimuthal coverage. We use the portion of FAZ data with effective full azimuth coverage as much as 10 km.**

Figure 6. **Rose diagram shows the offset and azimuthal coverage. We limit the crossline offset of the FAZ data to 4 km to simulate WAZ geometry.**

et al., 2001). The FAZ towed streamer data were acquired using multiple vessels and configurations designed to maximize azimuth variation while maintaining good offset distribution (F. Mandroux, 2012, personal communication). Although we have offsets greater than 10 km in this survey, we only use offsets 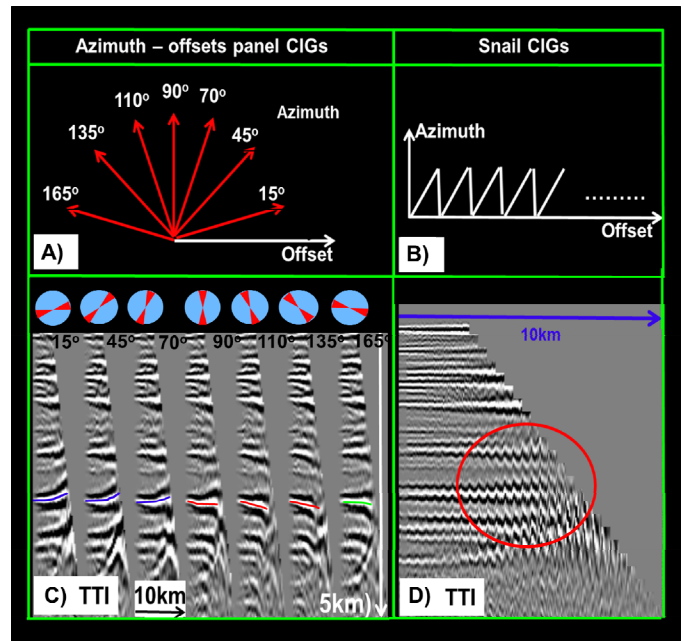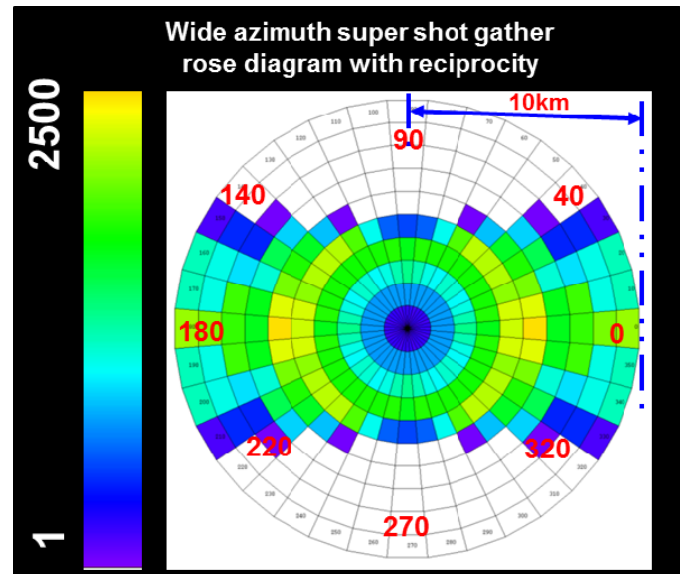less than 10 km for this study. Full azimuth coverage as much as 10 km with reciprocity is shown in a rose diagram (Fig. 4).

After the preprocessing sequences—noise attenuation, designature, and 3D surface related multiple elimination (SRME)—the FAZ data are divided into seven azimuth sectors (15°, 45°, 70°, 90°, 110°, 135°, 165°) by azimuth-offset binning (Fig. 5A). These seven sectors are migrated to produce the CIGs for multi-azimuth TTI tomographic joint inversion. After three iterations of TTI tomography, we still observe conflicting residual moveouts among azimuths near the folded areas. As azimuth changes from 15° to 165°, we observe the residual curvature gradually evolving from over-corrected to under-corrected, and then to flat, which indicates the need for different apparent velocities in each
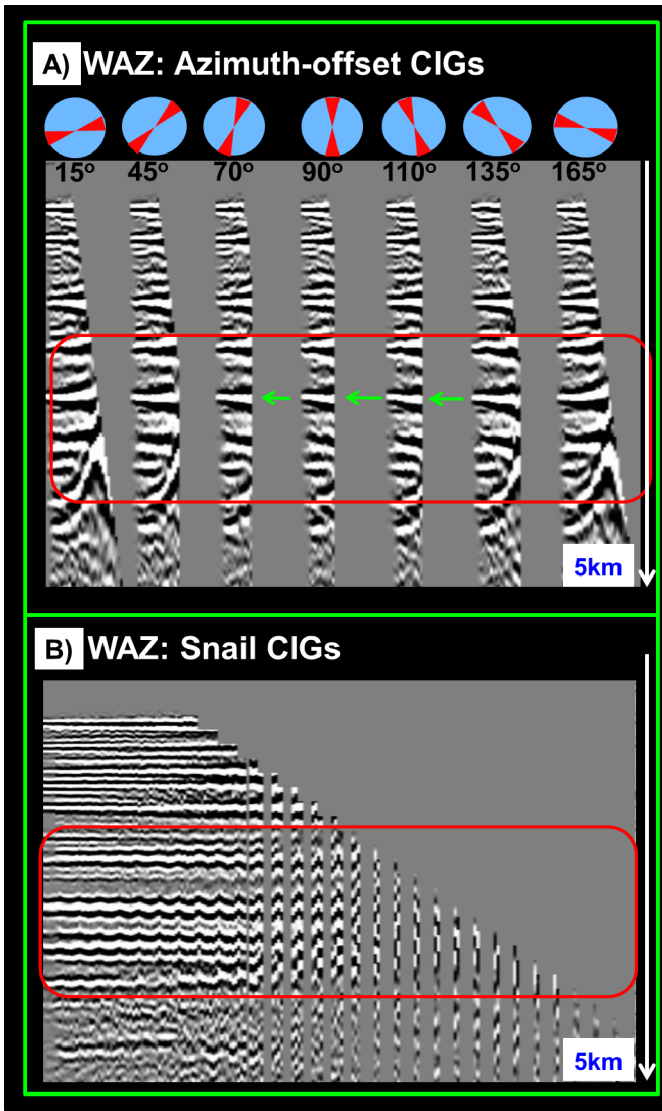
Figure 7. TTI Residual curvature with simulating WAZ geometry. (A) Azimuth-offset CIGs. Green arrows indicate where the azimuthal sectors lose the resolution for the CIG curvatures. (B) Snail CIGs.

Figure 8. (A) v_0 of TTI model. (B) v_0 of tilted orthorhombic model, which is simpler than TTI.

azimuth to flatten the gathers (Fig. 5C). We also sort the data into "snail" CIGs (Hung et al., 2006; Wombell 2006; Lecerf et al., 2009) as defined by Figure 5B, which show a distinct and significant wobbling effect in the snail CIGs (Fig. 5D). Clearly, both types of CIGs reveal the limitation of a TTI model in the presence of tilted orthorhombic anisotropy.

Effect of Azimuth for Detecting Tilted Orthorhombic Anisotropy

Here we discuss the effectiveness of FAZ versus WAZ for detecting the tilted orthorhombic effect in the overburden. We limit the crossline offset of the FAZ data to 4 km to simulate WAZ geometry. Figure 6 shows a rose diagram with the simulated WAZ geometry. Figure 7A shows that the WAZ lacks the resolution to detect inconsistent curvatures among azimuths for several azimuth sectors (marked by the green arrows). Although we still observe the wobbling effect in snail gathers with the simulated WAZ data (Fig. 7B), it is not as clear as the FAZ data (Fig. 5D) due to the absence of far offset in some azimuth sectors. Clearly FAZ has an advantage over WAZ in detecting tilted orthorhombic anisotropy. This also may explain how TTI might
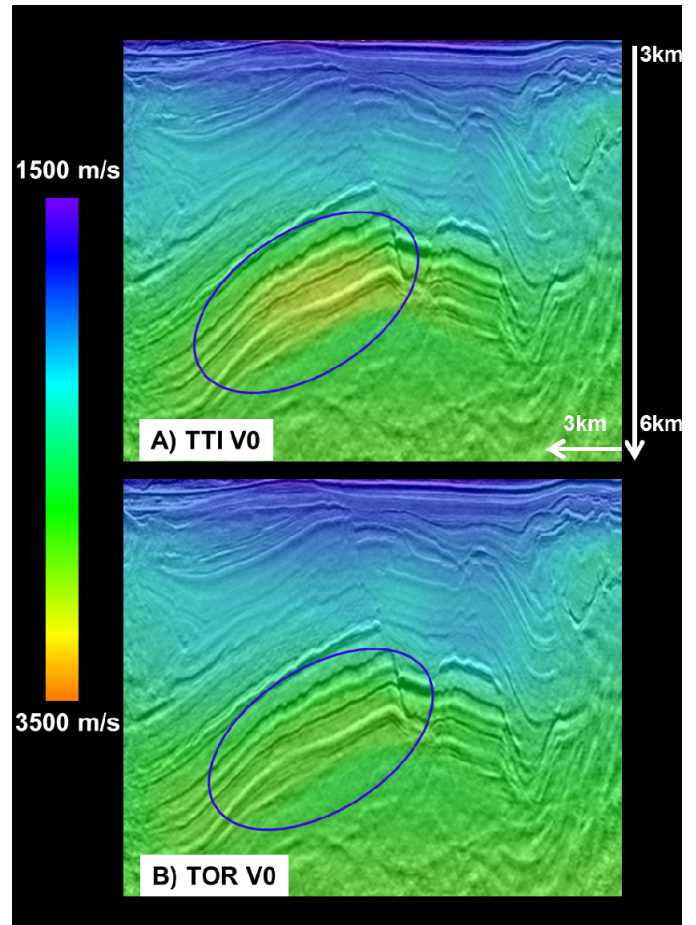
generate a reasonable model with WAZ data and unwittingly ignore the possible existence of orthorhombic anisotropy.

Tilted Orthorhombic Tomography of FAZ Data

For tilted orthorhombic model building, an initial velocity model is extracted from a smoothed velocity model with TTI tomography. Each of the seven azimuths is updated independently using TTI tomography to yield flat CIGs. The parameters of the individual TTI models are then converted to the initial set of orthorhombic parameters (v_0, ε_1, ε_2, δ_1, δ_2, δ_3, and α) as shown in Figure 2. Dip and azimuth models, θ and φ, are inherited from the TTI model building. After performing the TOR tomographic velocity update, we produced the final sediment model shown in Figure 8, where TOR tomography produces a smoother v_0 field than that of TTI, which shows a leakage of the azimuthal anisotropy components into the TTI velocity field. At a location near the faulted fold area (marked with a red star on Figure 9A), the direction of fast velocity is conformable with the inconsistent curvatures from CIGs shown in Figure 5C: TTI CIGs from the 15° azimuth are overcorrected more than those from other azimuths, indicating the azimuth is approximately the expected direction of fast velocity. The difference between ε_1 and ε_2, ranging from 0.03 to 0.06 (Fig. 9B), shows the strength of azimuthal anisotropy: the larger the difference, the stronger the orthorhombic anisotropic effect. Overall, we observe that the fastest velocity direction and the strength of azimuthal anisotropy ($\varepsilon_1 - \varepsilon_2$) are consistent with the geologic settings.

After three iterations of TOR tomographic updates, we observe that the gathers are both more consistent across azimuths and flatter overall with TOR imaging. Additionally, the wobbling effects in the snail gathers are greatly reduced (Figs. 10A
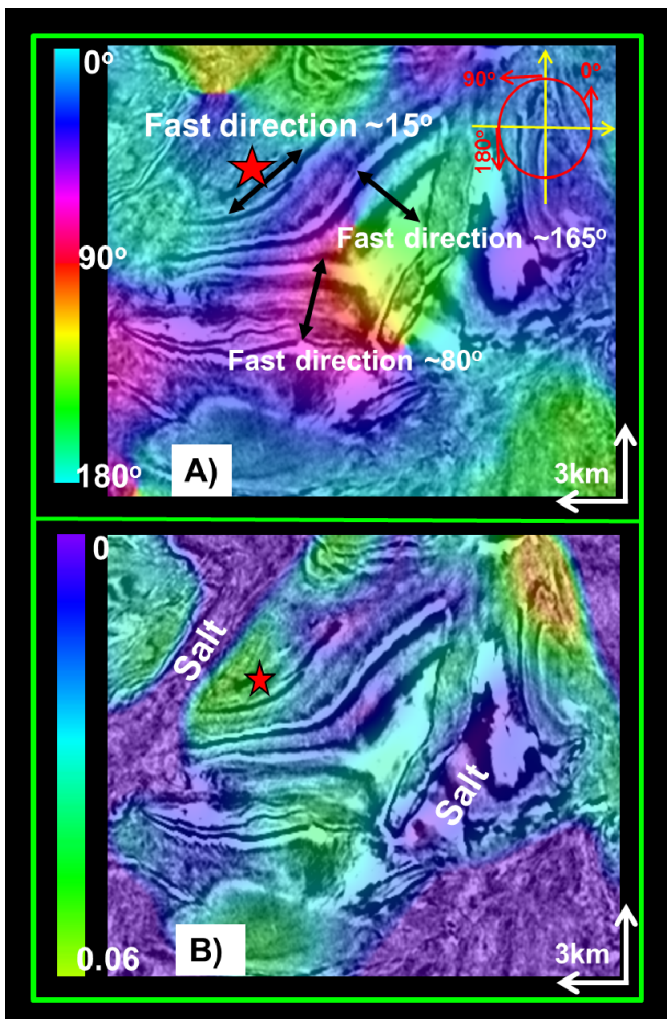
Figure 9. (A) Estimated fast velocity direction on the surface. (B) Azimuthal anisotropy ($\varepsilon_1 - \varepsilon_2$).

Figure 10. FAZ TOR tomography output. (A) TOR seven-azimuth panels and (B) TOR snail CIG.

and 10B). Figure 11 compares the salt body RTM image from TTI model building and TOR model building. In the suprasalt folded belt, TOR imaging improves the focusing of dipping events, the fold structure and fault positions. With this better definition of overburden, salt geometry is better imaged with the TOR model, which improves the focusing and event continuity in the subsalt area.

CONCLUSIONS

Recently available FAZ data in the Gulf of Mexico provide the abundant azimuthal information needed to derive a realistic anisotropy models to describe data for all azimuthal sectors, especially in the complex geology areas. Herein we define a TOR depth model building procedure utilizing the parameters from the azimuthal sectors and apply it to a complex Gulf of Mexico FAZ dataset. Compared to WAZ data, we observe that FAZ data are more effective in detecting and estimating azimuthal anisotropy in the overburden in the presence of fractures and uneven stress. Compared to TTI imaging, TOR imaging reduces the inconsistent residual curvatures in CIGs for all azimuths, provides better focusing of the structural events and improves imaging of the overburden mini-basins. Consequently, this has enabled us to improve the visualization of salt geometry and, hence, provide better subsalt images. Furthermore, the geological meaningfulness of the derived azimuthal anisotropy is supported by the observation that the fast velocity direction in the TOR model is consistent with the strikes of fractures in our study area.
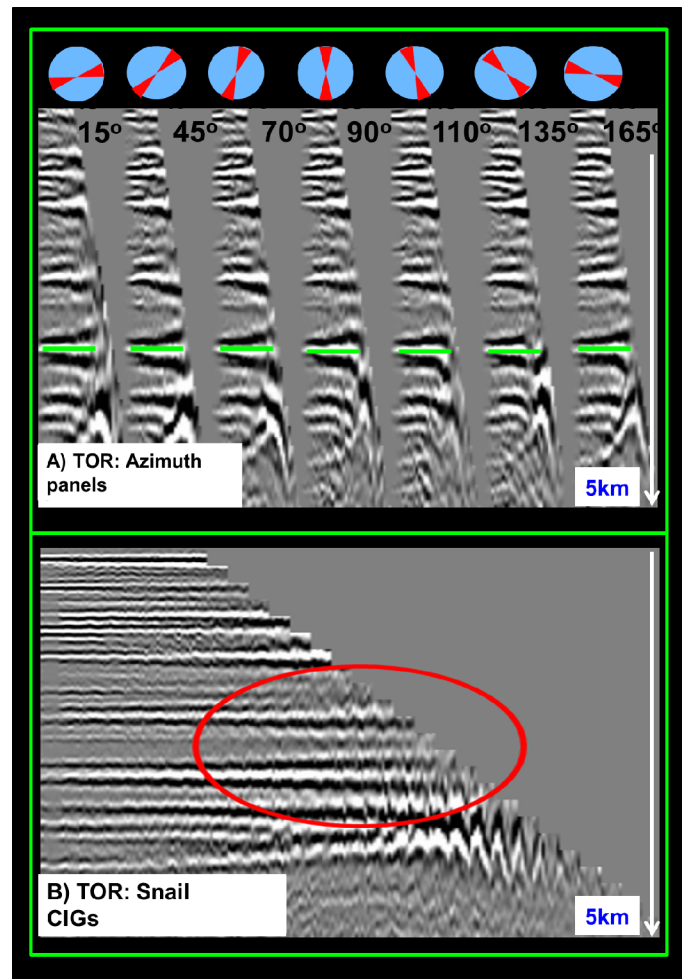
REFERENCES CITED

Alkhalifah, T., 2003, An acoustic wave equation for orthorhombic anisotropy: Geophysics, v. 68, p. 1169–1172, doi:10.1190/1.1598109.

Bakulin, A., V. Grechka, and I. Tsvankin, 2000, Estimation of fracture parameters from reflection seismic data—Part II: Fractured models with orthorhombic symmetry: Geophysics, v. 65, p. 1803–1817, doi:10.1190/1.1444864.

Birdus, S., J. Sun, W. Sun, Y. Xie, M. Gazzoli, M. Andreolli, and A. Ursulic, 2012, Multi-azimuth PSDM processing in the presence of orthorhombic anisotropy—A case history offshore northwest Australia: Society of Exploration Geophysicists Expanded Abstracts 2012, 5 p., doi:10.1190/segam2012-0538.1.

Bowling, J., S. Ji, D. Lin, D. Chergotis, B. Nolte, and D. Yanchak, 2010, Mad Dog TTI RTM: Better than expected: Society of Exploration Geophysicists Expanded Abstracts 2010, p. 3313–3317, doi:10.1190/1.3513536.

Cheadle, S. P., R. J. Brown, and D. C. Lawton, 1991, Orthorhombic anisotropy: A physical seismic modeling study: Geophysics, v. 56, p. 1603–1613, doi:10.1190/1.1442971.
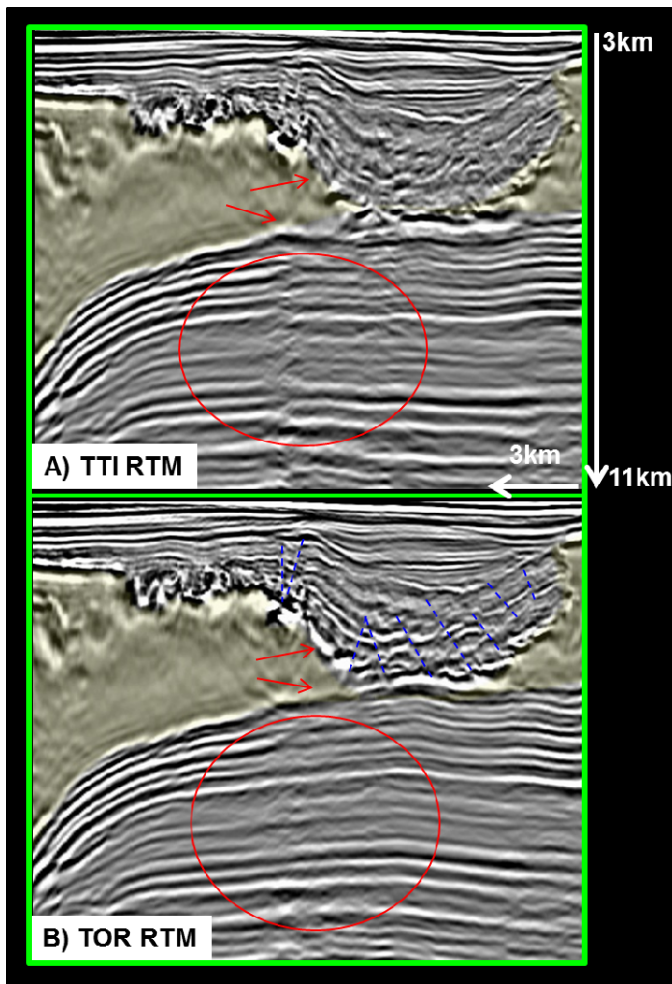
Figure 11. (A) FAZ TTI RTM salt body image. (B) FAZ TOR RTM salt body image. Blue dashed lines indicate faults. Yellow areas are salt.

Dewey, F., M. Meulen, and P. Whitfield, 2006, Using dual-azimuth data to image below salt domes: First Break, v. 24, p. 55–59, doi:10.3997/1365-2397.2006014.

Dickinson, D., and T. Ridsdill-Smith, 2010, Benefits of multi-azimuth depth migration over the Tidepole Field, North West Shelf, Australia: 72nd European Association of Geoscientists and Engineers Conference and Exhibition Extended Abstracts, <http://www.earthdoc.org/publication/publicationdetails/?publication=39144> Last accessed September 1, 2013.

Fowler, P. J., and R. King, 2011, Modeling and reverse time migration of orthorhombic pseudo-acoustic P-waves: Society of Exploration Geophysicists Expanded Abstracts 2011, p. 190–195, doi:10.1190/1.3627580.

Han, W., and S. Xu, 2012, Orthorhombic raytracing and traveltime calculation: 74th European Association of Geoscientists and Engineers Conference and Exhibition Extended Abstracts, <http://www.earthdoc.org/publication/publicationdetails/?publication=59224> Last accessed September 1, 2013.

Hilley, G. E., J. R. Arrowsmith, and L. Amoroso, 2001, Interaction between normal faults and fractures and fault scarp morphology: Geophysical Research Letters, v. 28, p. 3777–3780, doi:10.1029/2001GL012876.

Huang, T., Y. Zhang, H. Z. Zhang, and J. Young, 2009, Subsalt imaging using TTI reverse time migration: The Leading Edge, v. 28, p. 448, doi:10.1190/1.3112763.

Huang, T., S. Xu, and Y. Zhang, 2007, Anisotropy estimation for prestack depth imaging—A tomographic approach: Society of Exploration Geophysicists Expanded Abstracts 2007, p. 124–128, doi:10.1190/1.2792395.

Hung, B., F. M. Zhang, J. Sun, M. Stanley, and A. Osadchuk, 2006, An automated 3D method for azimuthal anisotropy analysis in marine seismic data: 68th European Association of Geoscientists and Engineers Conference and Exhibition Extended Abstracts, <http://www.earthdoc.org/publication/publicationdetails/?publication=400> Last accessed September 1, 2013.

Lecerf, D., S. Navion, J. L. Boelle, A. Belmokhtar, and A. Ladmek, 2009, Azimuthal residual velocity analysis in offset vector for WAZ Imaging: 71st European Association of Geoscientists and Engineers Conference and Exhibition Extended Abstracts, <http://www.earthdoc.org/publication/publicationdetails/?publication=24088> Last accessed September 1, 2013.

Li, Y. F., W. S. Han, C. S. Chen, and T. Huang, 2012, Velocity model building for tilted orthorhombic depth imaging: Society of Exploration Geophysicists Expanded Abstracts 2012, 5 p., doi:10.1190/segam2012-1231.1.

Lynn, H. B., and R. J. Michelena, 2011, Introduction to this special section: Practical applications of anisotropy: The Leading Edge, v. 30, p. 726–730, doi:10.1190/1.3609086.

Mensch T., V. Farra, L. de Sismologie, and S. C. Singh, 1998, 3D seismic traveltime tomography in orthorhombic media: Society of Exploration Geophysicists Expanded Abstracts 1998, p. 1863–1866, doi:10.1190/1.1820298.

Schoenberg, M., and K. Helbig, 1997, Orthorhombic media: Modeling elastic wave behavior in a vertically fractured earth: Geophysics, v. 62, p. 1954–1974. doi:10.1190/1.1444297.

Thomsen, L., 1986, Weak elastic anisotropy: Geophysics, v. 51, p. 1954–1996, doi:10.1190/1.1442051.

Tsvankin, I., 1997, Anisotropic parameters and P-wave velocity for orthorhombic media: Geophysics, v. 62, p. 1292–1309, doi:10.1190/1.1444231.

Williams, M., and E. Jenner, 2002, Interpreting seismic data in the presence of azimuthal anisotropy; or azimuthal anisotropy in the presence of seismic interpretation: The Leading Edge, v. 21, p. 771–774, doi:10.1190/1.1503192.

Wombell, R., 2006, Characteristics of azimuthal anisotropy in narrow-azimuth marine streamer data: 68th European Association of Geoscientists and Engineers Conference and Exhibition Extended Abstracts, <http://www.earthdoc.org/publication/publicationdetails/?publication=157> Last accessed September 1, 2013.

Xie, Y., S. Birdus, J. Sun, and C. Notfors, 2011, Multi-azimuth seismic data imaging in the presence of orthorhombic anisotropy: 73rd European Association of Geoscientists and Engineers Conference and Exhibition Extended Abstracts, <http://www.earthdoc.org/publication/publicationdetails/?publication=50384> Last accessed September 1, 2013.

Zhang, H., and Y. Zhang, 2011, Reverse time migration in vertical and tilted orthorhombic media: Society of Exploration Geophysicists Expanded Abstracts 2011, p. 185–189, doi: 10.1190/1.3627568.

Zhou, J., N. H. Ngoc, T. Borthwick, K. Zhao, and K. H. Teng, 2011, TTI/HTI anisotropy for fracture/faults image inside granite basement: 73rd European Association of Geoscientists and Engineers Conference and Exhibition Extended Abstracts, <http://www.earthdoc.org/publication/publicationdetails/?publication=50202> Last accessed September 1, 2013.

Zhu, Y., and L. Tsvankin, 2007, Plane-wave attenuation anisotropy in orthorhombic media: Geophysics, v. 72, p. D9–D19, doi:10.1190/1.2387137.